New Insights into Bonding in Phase-Change Materials from Ion-Driven Synthesis

Zhen Zhang[a], Xuanguang Zhang[a], Bin Liu [b, c], Jian Zhou[a], Stephen R. Elliott[d] and Zhimei Sun[a*]

[a] *School of Materials Science and Engineering, Beihang University, Beijing 100191, China*
[b] *National Key Laboratory of Spintronics, Hangzhou International Innovation Institute, Beihang University, Hangzhou 311115, China.*
[c] *State Key Laboratory of Materials for Integrated Circuits, Shanghai Institute of Microsystem and Information Technology, Chinese Academy of Sciences, 865 Changning Road, Shanghai 200050 China.*
[d] *Department of Chemistry, University of Cambridge, Cambridge, CB2 1TQ, UK*
[*]Corresponding author: Zhimei Sun (zmsun@buaa.edu.cn).

1. Experimental Section

1.1 Materials

All the chemicals used were of analytical grade: tellurium (Te) 99.99% purity, antimony trichloride ($SbCl_3$) 99% purity, tin chloride ($SnCl_4$) 99% purity， bismuth chloride ($BiCl_3$) 99% purity，yttrium nitrate ($Y(NO_3)_3$) 99.9% purity，scandium nitrate ($Sc(NO_3)_3$) 99.9% purity，potassium hydroxide (KOH) ≥95% purity，ethylene glycol ($C_2H_6O_2$) ≥99.5% purity, ethanol absolute ≥ 99.5% purity were obtained from Shanghai Macklin and were used as received, without further purification. Deionized water was employed throughout the study.

1.2 Iono-reaction-based synthesis of PCMs

20 mmol $SbCl_3$ (or $BiCl_3$, $SnCl_2$) was dispersed in 30 ml of ethylene glycol, obtaining dispersion A. In a separate container, 60 mmol of Te powder (needle crystals) was

mixed in 40 ml of ethylene glycol and the mixture was stirred for 30 minutes, obtaining dispersion B. Dispersions A and B were mixed, and then 120 mmol of KOH was added. The reactants were stirred for 1 hour before transferring them to a tetrafluoroethylene-lined stainless-steel reactor. The reaction condition was maintained at a constant temperature of 200 °C for 24 hours. Later, the reactor was allowed to cool to room temperature naturally, and the reaction products were then collected. The collected products were washed alternately with deionized water and absolute ethanol until the pH reached neutrality. Finally, the products were dried in a vacuum at 60 °C to obtain the crystalline PCM samples.

1.3 Structural characterization

The morphologies of the Sb_2Te_3 nanosheets were analyzed using field emission scanning electron microscopy ((FESEM, JEOL JSM7001F), equipped with energy-dispersive spectroscopy (EDS) The crystalline phase identification and lattice parameters were determined through X-ray diffraction (XRD, Rigaku-D MAX-2550PC diffractometer using Cu Kα radiation with scanning steps of 0.02°). The bonding states of different elements were analyzed using X-ray photoelectron spectroscopy (XPS, Phi 5000, ULVAC Phi).

1.4 Computational Methods

The first-principles calculations for Electron Localization Function (ELF), band structure, Crystal Orbital Hamilton Population (COHP) and Crystal Orbital Bond Index (COBI) analyses in this work were performed using the projected augmented wave method (PAW) with GGA-PBE-based pseudopotentials,[1] as implemented in the ab

initio Simulation Package (VASP).[2] The GGA-PBE theory level was used for structure optimization and describing the electronic structure. An energy cutoff of 300 eV was used to truncate wavefunctions and solve the Kohn Sham equations. In structural optimization, an energy convergence criterion of 10^{-8} eV was used. The ionic forces were converged with a convergence criterion of -0.01 eV. A gamma-centered *k*-point mesh of 9 × 9 × 1 was used for Sb_2Te_3 and Bi_2Te_3, and 5 × 5 × 5 was used for SnTe. Cell parameters were allowed to relax (resulting in $a = b = 4.304$ Å, $c = 31.777$ Å for trigonal Sb_2Te_3, $a = b = 4.418$ Å, $c = 32.257$ Å for trigonal Bi_2Te_3 and $a = 6.351$ Å for cubic SnTe).

The COHP and COBI analyses were performed with the Lobster code, upon a transformation of the (plane) wave functions from VASP into a localized basis set (STO). (16,36,37,42,43) [https://pubs.acs.org/doi/full/10.1021/jp202489s]

The atom-in-molecules (AIM) analysis was performed using the CP2K code [3] and Multiwfn. CP2K is based on a mixed Gaussian basis set with an auxiliary plane-wave basis set (GPW).[4] Periodic-boundary conditions for the simulation box, with $a = b = 4.304$ Å, $c = 31.777$ Å for trigonal Sb_2Te_3, $a = b = 4.418$ Å, $c = 32.257$ Å for trigonal Bi_2Te_3 and $a = 6.351$ Å for cubic SnTe, were enforced in the calculations. All elements were represented using a double-ζ valence-polarized (DZVP) Gaussian basis set,[5] in conjunction with the Goedecker-Teter-Hutter (GTH) pseudopotential[6] in the Generalized Gradient Approximation (Perdew–Burke–Ernzerhof exchange-correlation functional[7]).

[1] Perdew, John P., Kieron Burke, and Matthias Ernzerhof. *Physical review letters*. **1996**, *77*, 3865.

[2] Kresse, Georg, and Jürgen Hafner. *Physical review B*. **1993**, *47*, 558.

[3] T. D. Kuhne, M. Iannuzzi, M. Del Ben, V. V. Rybkin, P. Seewald, F.Stein, T. Laino, R. Z. Khaliullin, O. Schutt, F. Schiffmann, D. Golze, J. Wilhelm, S. Chulkov, M. H. Bani Hashemian, V. Weber, U. Borštnik, M. Taillefumier, A. S. Jakobovits, A. Lazzaro, H. Pabst, T. Muller, R. Schade, M. Guidon, S. Andermatt, N. Holmberg, G. K. Schenter, A. Hehn, A. Bussy, F. Belleflamme, G. Tabacchi, et al., *J. Chem. Phys.* **2020**, *152*, 194103.

[4] J. VandeVondele, M. Krack, F. Mohamed, M. Parrinello, T. Chassaing, J. Hutter, *Comput. Phys. Commun.* **2005**, *167*, 103.

[5] J. VandeVondele, J. Hutter, *J. Chem. Phys.* **2007**, *127*, 114105.

[6] S. Goedecker, M. Teter, J. Hutter, *Phys. Rev. B* **1996**, *54*, 1703.

[7] J. P. Perdew, K. Burke, M. Ernzerhof, *Phys. Rev. Lett.* **1996**, *77*, 3865.

2. Characterization of the experimental synthesis products and reaction progression.

We conducted elemental analyses on typical samples obtained at different reaction times to further elucidate the progress of the reaction.

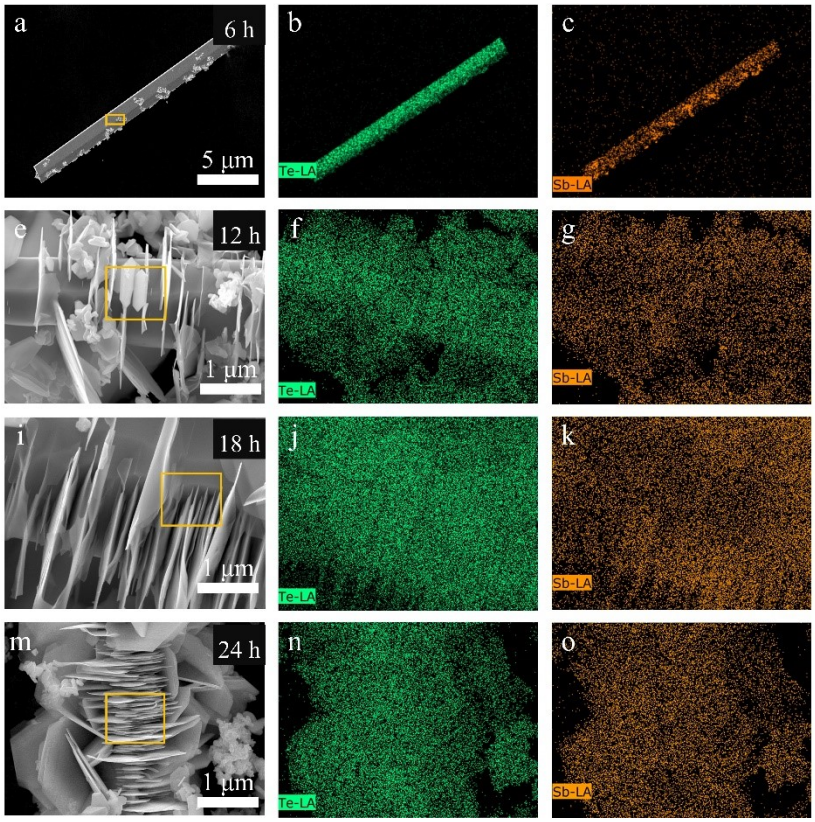

d

Element	at.%	Error %
Sb	5.2	0.32
Te	94.8	1.31

h

Element	at.%	Error %
Sb	20.7	0.94
Te	79.3	1.44

l

Element	at.%	Error %
Sb	32.6	1.25
Te	67.4	1.50

p

Element	at.%	Error %
Sb	38.2	1.39
Te	61.8	1.40

Figure. S1. Elemental mapping and distribution of the Sb_2Te_3 products obtained at 6, 12, 18, and 24 hours after the beginning of the reaction.

Through validation of Te-related compounds during the reaction, we obtained an accurate chemical pathway for Te.

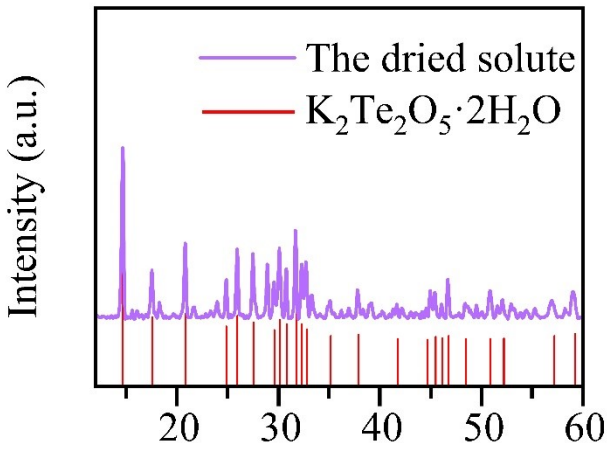

Figure. S2. The XRD pattern of dried byproducts from the dispersion.

After drying and purifying the solute from the post-reaction suspension, the obtained product was primarily composed of $Na_2Te_2O_5 \cdot 2H_2O$, with tellurium in the +4 oxidation state. This result is consistent with our predicted disproportionation reaction outcome.

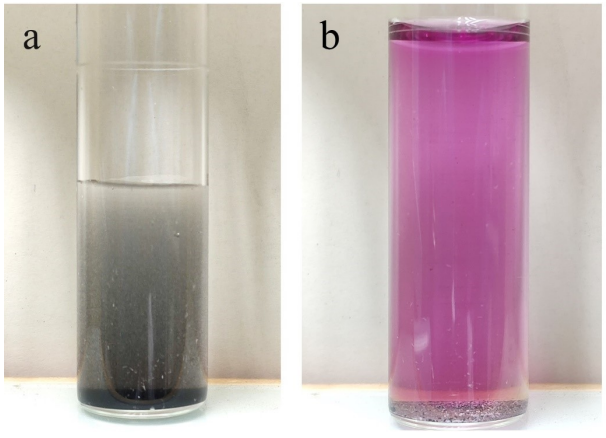

Figure. S3. Disproportionation of tellurium powder in KOH solution: a) The suspension obtained by dispersing tellurium powder in ethylene glycol; b) After the addition of KOH, the tellurium powder dissolved and exhibited a purple Te^{2-} solution.

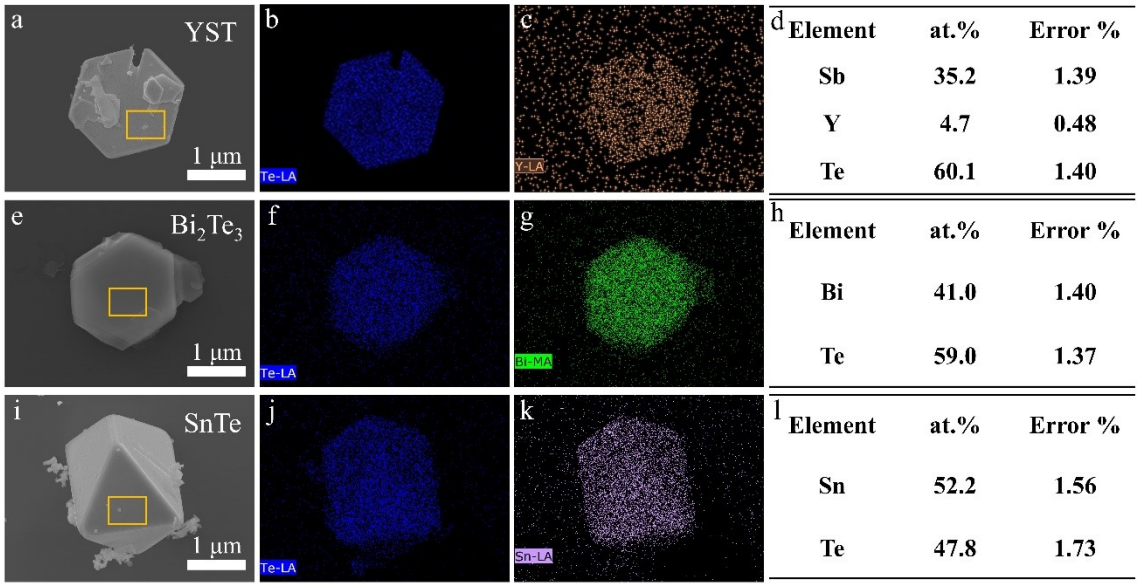

d Element	at.%	Error %
Sb	35.2	1.39
Y	4.7	0.48
Te	60.1	1.40

h Element	at.%	Error %
Bi	41.0	1.40
Te	59.0	1.37

l Element	at.%	Error %
Sn	52.2	1.56
Te	47.8	1.73

Figure. S4. Elemental mapping and distribution of: Y-doped Sb_2Te_3 (a-d); Bi_2Te_3 (e-h); SnTe (i-l).

To experimentally investigate whether there is polarization/ionicity in the Te-M-Te bonding, Sb_2Te_3 was doped with two trivalent metal elements, Y and Sc (i.e., $Y_{0.2}Sb_{1.8}Te_3$ and $Sc_{0.2}Sb_{1.8}Te_3$, Figure S5). Variations in the XRD patterns were observed in doped Sb_2Te_3. Not only were there differences in the positions of the main peaks, but notably, the Sc-ST sample exhibits a prominent (0 0 15) diffraction peak - which remains barely detectable in both Sb_2Te_3 and Y-ST samples. This peak has become the main peak in Sc-ST, indicating a fundamental alteration in crystal growth orientation) indicating differences in crystal-growth orientation, but also the same peak (0 1 5) exhibited a shift among different materials. According to the Bragg equation, the shift suggests alterations of interplanar spacings within the crystalline PCMs due to the presence of the dopants. The variation in lattice constants was evidently due to the

differing radii of the dopant atoms (Y, Sc) compared to Sb, but it is also correlated with their bonding patterns, as the covalent and ionic radii of the same element may vary. Therefore, of greater interest to us were the relative positions of the main XRD peaks, which follow the order of Y < Sb ≈ Sc. This observation implied an actual ionic-radius sequence of Y (90.0 pm) > Sb (76.0 pm) ≈ Sc (74.5 pm) within the lattice of the material, closely matching their respective ionic radii, but challenging to rationalize through variations in covalent radii (**Table S1**). These findings further highlighted the prevalence of ionicity in M-Te type PCMs, indicating that the charge transfer inherent in hypervalent bonding does indeed exist within PCMs and could be directly observed.

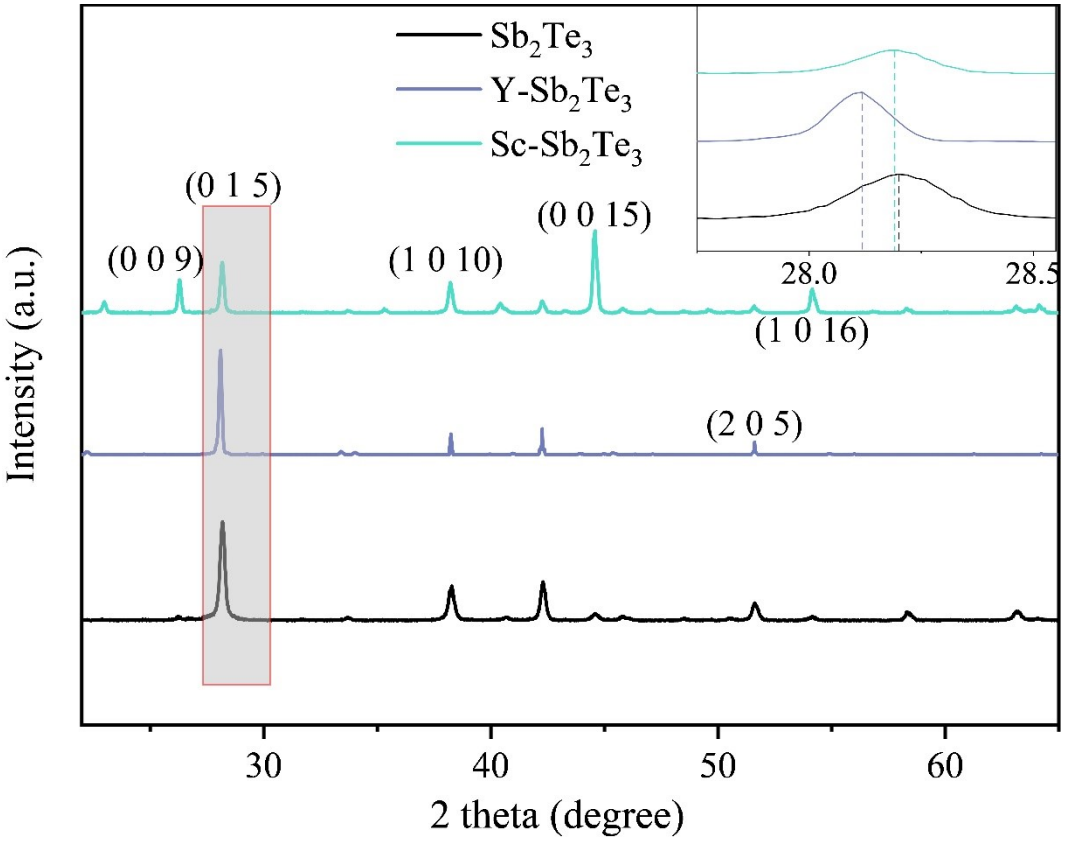

Figure. S5. XRD patterns of crystalline Sb_2Te_3 and Y/Sc-doped crystalline Sb_2Te_3. The main peak at ~28 deg is boxed and magnified in the top right corner.

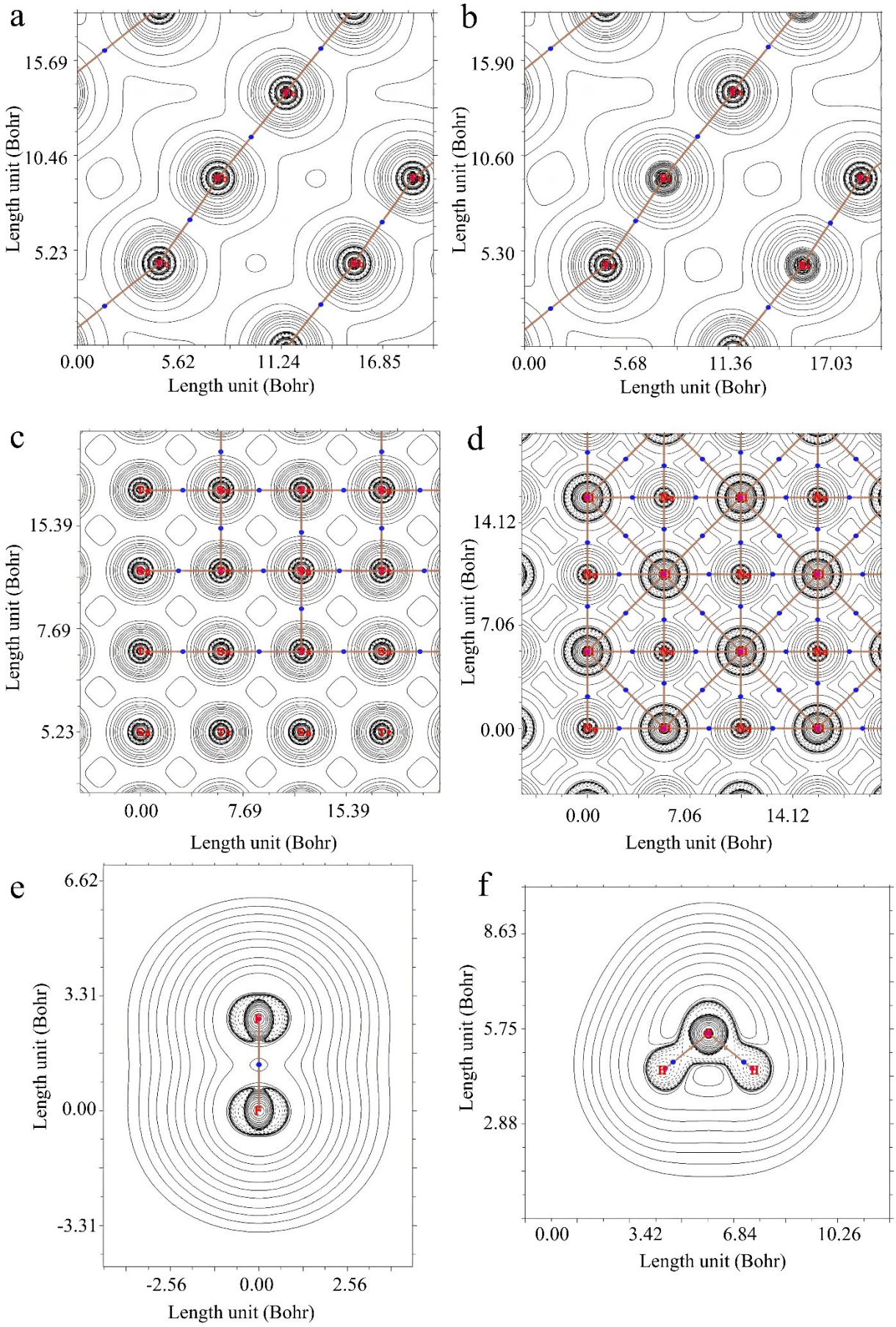
a
15.69
10.46
5.23
Length unit (Bohr)
0.00
5.62
11.24
16.85
Length unit (Bohr)
b
15.90
10.60
5.30
Length unit (Bohr)
0.00
5.68
11.36
17.03
Length unit (Bohr)
c
15.39
7.69
5.23
Length unit (Bohr)
0.00
7.69
15.39
Length unit (Bohr)
d
14.12
7.06
0.00
Length unit (Bohr)
0.00
7.06
14.12
Length unit (Bohr)
e
6.62
3.31
0.00
-3.31
Length unit (Bohr)
-2.56
0.00
2.56
Length unit (Bohr)
f
8.63
5.75
2.88
Length unit (Bohr)
0.00
3.42
6.84
10.26
Length unit (Bohr)

Figure S6. The Laplacian value maps of different materials: (a) Sb_2Te_3; (b) Bi_2Te_3; and (c) SnTe. (d) NaCl. (e) F_2. (f) H_2O.

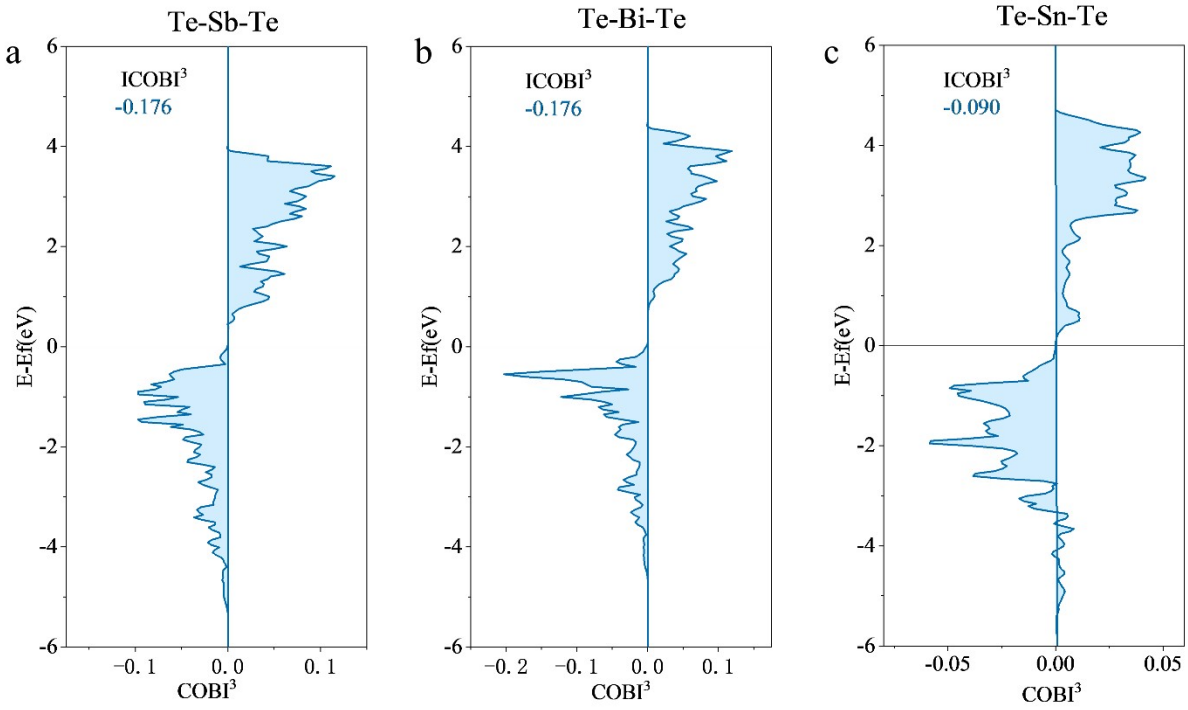

Figure S7. $ICOBI^3$ plots of crystalline: (a) Te-Sb-Te; (b) Te-Bi-Te; and (c) Te-Sn-Te.

Table S1. Covalent and ionic radii of the elements Y, Sb, and Sc.[5]

	Y	Sb	Sc
covalent radius (pm)	163	140	148
ionic radius (pm)	90.0	76.0	74.5

Table S2. The electronegativity values of Te, Sb, Bi, Sn.

	Te	Sb	Bi	Sn

electronegativity	2.10	2.05	2.02	1.96